Available online at www.sciencedirect.com

ScienceDirect

Procedia CIRP 115 (2022) 30–35

www.elsevier.com/locate/procedia

10th CIRP Global Web Conference – Material Aspects of Manufacturing Processes

Identification of material properties for finite element simulation of the deep rolling process applied to welded joints

Steffen Heikebrügge[a,*], Bernd Breidenstein[a], Benjamin Bergmann[a], Christian Dänekas[b], Peter Schaumann[b], Jan Schubnell[c]

[a]*Institute of Production Engineering and Machine Tools, Leibniz University Hannover, An der Universität 2, 30823 Garbsen, Germany*
[b]*Institute for Steel Construction, Leibniz University Hannover, ForWind, Appelstrasse 9A, 30167 Hannover, Germany*
[c]*Fraunhofer Institute for Mechanics of Materials IWM, 79108 Freiburg, Germany*

* Corresponding author. Tel.: +49-511-762-18293; Fax: +49-511-762-18293. *E-mail address:* heikebruegge@ifw.uni-hannover.de

Abstract

During butt welding of structural steels, an inhomogeneous material state across the weld occurs that has a detrimental influence on fatigue strength. In the presented study, the identification of Lemaitre Chaboche elastoviscoplastic model parameters is shown. The identification was conducted for base material, heat affected zone and filler material of submerged arc butt welded 1.8813 (S355MLO) structural steel. The derived constitutive model was integrated into a finite element simulation of the deep rolling process, which has not been investigated before for the post treatment of welded joints. Mechanical process loads were derived, giving first explanations of the deformation behavior.

Keywords: Constitutive model; finite element simulation; deep rolling; welded joints; residual stress

1. Introduction

Fixed offshore wind turbine support structures are mostly designed as monopiles. These monopiles consist of steel segments that are joined by submerged arc welding. During the welding process, geometrical and metallurgical notches are created at the transition from base material to filler material. This transition is called the weld toe. Depending on the welding process, the weld toe is characterized by a more or less pronounced heat affected zone whose mechanical properties significantly differ from the ones of base or filler material [1]. The combination of geometrical and metallurgical notches together with a possible detrimental residual stress state leads to a comparably lower fatigue resistance than the one of pure base material. As a result, wall thicknesses of welded components are designed accordingly. To overcome this issue, different post weld treatment methods such as burr grinding, tungsten inert gas welding or high frequency mechanical impact treatment were developed to improve the fatigue strength of welded joints [2,3]. These methods aim at either reducing the stress concentration by influencing the weld toe geometry or additionally at inducing beneficial subsurface properties such as compressive residual stresses. One mechanical surface treatment process that has not been investigated in detail before for the application to welded joints is hydrostatic deep rolling. The positive influence of deep rolling on surface and subsurface properties and the fatigue resistance of structural parts was proven numerously in the past [4].

For an effective treatment of the welded joint regarding a fatigue strength enhancement, the deep rolling process has to influence the fatigue critical weld toe. For being able to predict

2212-8271
10.1016/j.procir.2022.10.045

the deformation behavior of the weld toe, finite element simulations of the deep rolling process can be utilized.

Current investigations focus on the derivation of so-called process signatures that are linked with the process parameters for the correlation between the acting material stress and the resulting material modification using the finite element (FE) method [5,6]. Effective variables in the workpiece are, for example, the von Mises equivalent stress acting in the depth profile or the elastoplastic equivalent strain. These are linked via the process signature with the resulting residual stress state or the generated plastic strain in order to determine necessary process variables and finally process parameters. This enables function-oriented process planning.

One prerequisite for correct numerical simulation of the deep rolling process is the constitutive behavior of the material. Due to the repeated plastic deformations of surface and subsurface during the deep rolling process, the hardening behavior must be known. This is especially due to the fact that the hardening behavior is responsible for the calculation of the amount fatigue relevant residual stresses after repeated plastic deformations. Numerical simulations of different post-treatment processes applied to welded joints have shown that knowledge of the constitutive behavior of base material, heat-affected zone and filler material must be available [7]. This ensures a correct representation of the deformation mechanisms and the induction of surface and subsurface properties as a result of the mechanical processing [1,8]. Accordingly, this requirement also applies to a numerical simulation of the deep rolling process applied to welded joints.

For the simulation of the deep rolling process, different constitutive models were used in the past. This includes the strain-rate dependent hardening model according to Johnson-Cook [9] or pure isotropic hardening models [10]. The elastoviscoplastic constitutive model according to Lemaitre and Chaboche (LC) that includes combined hardening was used most frequently [5,6,11].

1.1. Constitutive model acc. to Lemaitre and Chaboche

The constitutive model used in this study combines the possible hardening mechanisms of isotropic and kinematic hardening that occur in metals during repeated plastic deformation. Both hardening mechanisms can occur accordingly during the deep rolling process. The model is based on the following constitutive equations, presented incrementally for uniaxial loading [12]:

Elastic and plastic components are represented by an additive decomposition of the total strain:

$$\mathrm{d}\epsilon = \mathrm{d}\epsilon_{el} + \mathrm{d}\epsilon_{pl} \tag{1}$$

In the elastic region, Hooke's law with Young's modulus E is valid. Yielding, i.e. the plastic range, is reached when the stress exceeds the local material yield strength σ_F. Otherwise, the material behaves elastically. For metals, especially under multi-axial loading, the yield criterion f according to von Mises is used.

The isotropic strain hardening, i.e. the increase of the yield surface, is defined by Zaverl & Lee [13] with the strain hardening function r, where Q defines the saturation value of the isotropic fraction, b the rate to saturation and p the accumulated plastic strain [14]:

$$\mathrm{d}r(p) = b(Q - r)\mathrm{d}p \tag{2}$$

The non-linear kinematic hardening according to Frederick and Armstrong [15] is represented for the uniaxial case via a back stress term x. Chaboche [16] has extended the back stress term to the effect that it can consist of several components $i = 1, 2, 3, ...n$. This allows the non-linear kinematic hardening behavior (Bauschinger effect) observed in cyclic material tests to be depicted more accurately than with only one component:

$$\mathrm{d}x = \sum_{i}^{n} \mathrm{d}x_i\,, \qquad \mathrm{d}x_i = C_i\mathrm{d}\epsilon_{pl} - \gamma_i x_i \mathrm{d}\epsilon_{pl} \tag{3}$$

The constants C and γ describe the saturation value of the back stress to C/γ and γ itself the rate to saturation. Here, C corresponds to the strain hardening modulus of kinematic strain hardening and γ to the rate at which the strain hardening modulus C decreases with increasing plastic strain.

The two components for isotropic and non-linear kinematic hardening are used to supplement the von Mises yield criterion f:

$$f = |\sigma - x| - r(p) - \sigma_F \tag{4}$$

As such, the stress increment resulting from uniaxial loading can be calculated as follows:

$$\mathrm{d}\sigma = E\left(1 - \frac{E}{E + \sum_i\left(C_i - \mathrm{sign}(\mathrm{d}\epsilon)\gamma_i x_i\right) + b(Q - r)}\right)\mathrm{d}\epsilon \tag{5}$$

With knowledge of the extended yield criterion and the possibility to calculate the stress increment, the constants b and Q of the isotropic hardening term as well as the constants C_i and γ_i can be determined in a numerical optimization. This requires cyclic material tests.

A numerical simulation of the deep rolling process on welded joints with an initially inhomogeneous surface and subsurface state has not been carried out so far. Numerical simulations of the process are necessary to explain the development of surface and subsurface properties in the geometrically and metallurgically inhomogeneous weld toe: Complete information about acting mechanical stresses cannot be obtained exclusively by analytical considerations or experimental investigations due to the irregular contact conditions between the rolling ball and the weld toe. A correct depiction of the constitutive behavior of base material (BM), heat affected zone (HAZ) and filler material (FM) is therefore crucial.

2. Derivation of LC constitutive model parameters

The investigated welded joints were created by six layer submerged arc welding of large metal sheets (2,200 x 600 x 19 mm³) made of 1.8813 (S355MLO) structural steel in an industrial environment. Layer dependent welding parameters are not presented for the sake of brevity. The filler material used was S2MoTiB. An exemplary cross section of the welded joint is shown in Fig.1.

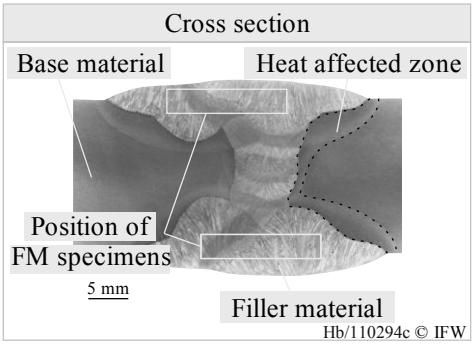

Fig. 1. Cross section of investigated welds

During the welding process, temperature measurements using type K thermocouples have been conducted in the vicinity of the weld toe, see top of Fig. 2. A detail of the resulting cross section and an exemplary hardness map are shown at the bottom of Fig. 2.

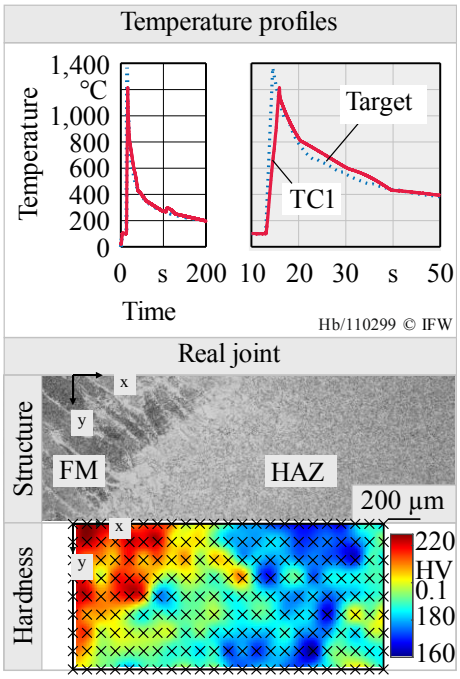

Fig. 2. Temperature profiles, detail of microstructure and hardness map

The filler material has a hardness of 220 HV0.1 whereas the HAZ shows a slight gradient of hardness in x-direction. This gradient decreases from 200 HV0.1 to 160 HV0.1. The bulk average of the hardness of the HAZ is approx. 190 HV0.1 (turquoise areas in hardness map).

To conduct cyclic material tests for the derivation of constitutive parameters, four round specimens were extracted from BM and two flat specimens from FM (along the welding direction, shown in Fig. 1). The final specimen geometries are shown in Fig. 3.

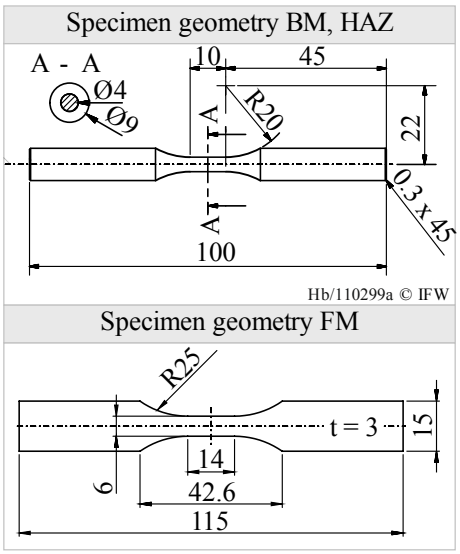

Fig. 3. Specimen geometries

For being able to depict the material behavior of the HAZ, four round bars with a diameter of 9 mm were extracted from base material of large metal sheets. The round bars were subjected to a thermomechanical simulation using a Gleeble® 3150 by Dynamic Systems Inc. The aim was to depict the real HAZ concerning the mechanical properties as well as hardness and microstructure. Therefore, the temperature profile measured during the welding process (Target) shown at the top of Fig. 2 was simulated and controlled by a thermocouple (TC1). As shown in Fig. 2, the course of TC1 matches the course of the target temperature course: The t8/5 times (cooling time from 800 °C to 500 °C) are 13.5 s for target and 15.8 s for TC1. With an average hardness of 192 HV0.1 of the gleeble HAZ the bulk hardness of the HAZ of the real specimens is matched, see Fig. 4. By optical characterization, the microstructure of the Gleeble HAZ specimen matches the microstructure of the real specimens as well, see Fig. 4.

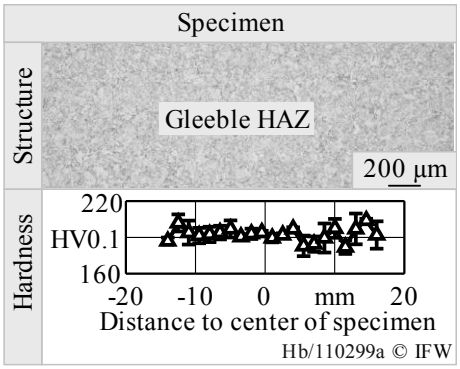

Fig. 4. Structure and hardness of Gleeble specimens

With the extracted specimens, uniaxial strain controlled material tests were carried out. For the BM and HAZ specimens, tests with maximum strain amplitudes of $\varepsilon_a = 2.0\%, 7.0\%$ at a strain rate of $\dot{\varepsilon}_a = 0.001$ 1/s were applied. With the FM specimens, incremental step tests at a frequency of $h = 0.5$ Hz with maximum strain amplitudes of $\varepsilon_a = 0.5\%, 1.0\%$ were conducted. For FM specimens lower

strain amplitudes were chosen due to possible buckling that occurred during testing at higher amplitudes.

The constitutive equations (1)–(5) presented in the introduction were implemented into the mathematic-statistical software SciLab. In a numerical optimization procedure the LC constitutive model parameters Q and b for isotropic hardening and C_i and γ_i for kinematic hardening were calibrated. The model was chosen to contain two backstresses. For the calibration of BM and HAZ constitutive model parameters the first 3 cycles of the strain controlled tests were used. For the calibration of FM, the first three cycles of the incremental step tests were used. Both lower maximum strain amplitudes were used for a validation of the parameters shown in Table 1 by an uniaxially strained single element model.

Table 1. Derived LC constitutive model parameters

	σ_F	Q	b	C_1	C_2	γ_1	γ_2
Material state	[MPa]	[MPa]	[-]	[MPa]	[MPa]	[-]	[-]
BM	400	35	4	5175	6459	3011	83
HAZ	350	63	1	30766	3986	221	88
FM	450	-194	543	212576	1092	12001	453

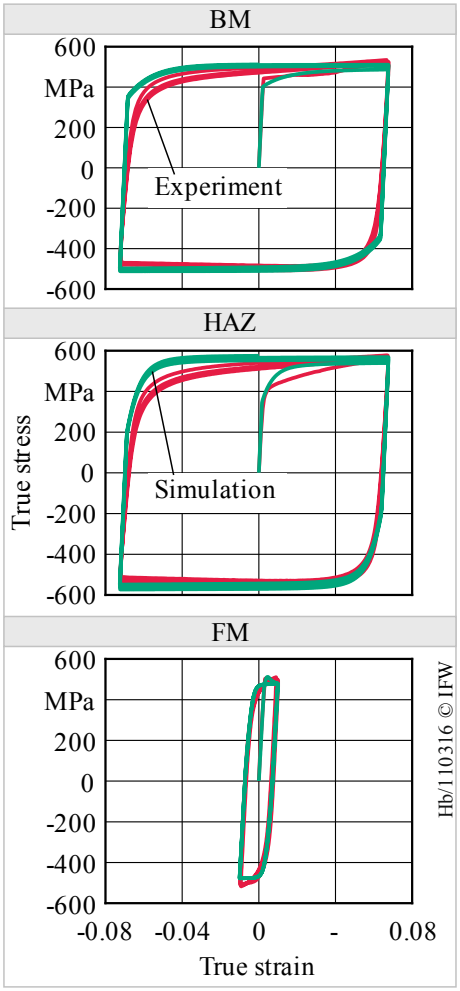

Fig. 5. Stress-strain hystereses of different material states

Young's modulus was set to E = 205 GPa for BM and HAZ specimens and 170 GPa for FM. In Fig. 5 experimentally and numerically determined stress-strain hystereses are shown. As it can be seen, hardening occurs differently between BM, HAZ and FM, with eg. HAZ showing higher max. stress values that are reached earlier than at BM.

3. FE simulation of the deep rolling process

3.1. Pre-processing of FE models

The derived parameters were implemented into a FE simulation of the deep rolling process. Simulations were conducted using Abaqus/Explicit 2017 by Dassault Systèmes. Specimens were modeled with a parametric CAD model that is based on the geometry of real specimens, see Fig. 1 and Fig. 6. Real specimens were measured by laser line scanning and evaluated using an algorithm implemented in the mathematical-statistic software MATLAB. For first simulations, the median of the local weld toe geometry was implemented (toe radius ρ = 0.83 mm, flank angle θ = 33.4°). Partitions of the model were integrated to depict the BM, HAZ and FM based on cross sections, see Fig. 1. Ceramic balls were modeled as ideally stiff due to their comparably high Young's modulus (approx. 315 GPa) and compressive strength (approx. 2,500 MPa). For simulations with smaller ball diameters (d_b = 2.2, 3.175 mm) of tools HG2 and HG3, an eighth model of the joint was used. For simulations with a bigger ball diameter (d_b = 12.7 mm) of tool HG13 a quarter model was used. Both models were constrained to a fixed support at the bottom face. Geometric nonlinearity was taken into account.

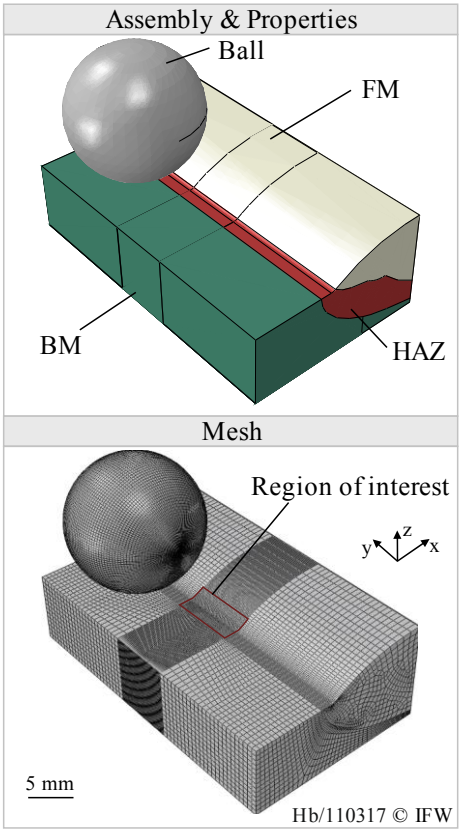

Fig. 6. Exemplary FE model used in simulations with HG13 tool

The mesh type used was C3D8R. In the region of interest, edge lengths of the meshes were chosen to be x = 50 µm,

y = 50 µm, z = 50 µm for the HG2 tool, x = 90 µm, y = 50 µm, z = 50 µm for the HG3 tool and x = y = z = 100 µm for the HG13 tool. The contact was modeled according to the friction law of Coulomb with a coefficient of friction of $\mu = 0.01$, calculated from process force measurements during deep rolling using the ratio of feed force F_f to rolling force F_r.

In a first step to describe the deformation behavior of the welded joints, a simple linear single track was simulated along the weld toe. Rolling speed was chosen to 5 m/min. The rolling forces derived from measurements are shown in Table 2.

Table 2. Measured process forces F_r [N] used in simulations

Rolling pressure p_r [MPa]	Ball diameter d_b [mm]		
	2.2	3.175	12.7
	Process force F_r [N]		
10	22.9	58.4	906.0
30	63.5	173.2	2477.0
40	83.3	231.4	3405.0

3.2. Post-processing: Derivation of mechanical process loads

For being able to understand the deformation behavior of the welded joint during deep rolling, acting mechanical process loads must be known. Due to support effects of the filler material, deformation of BM, HAZ and FM takes place simultaneously. In a first step, the mechanical process loads are described as the locally acting von Mises stresses in the region of interest. As the filler material supports the ball during the process, an evaluation of the mechanical process loads in BM/HAZ and FM is necessary. This was done by two paths that point normal from the center point of contact, see Fig. 7.

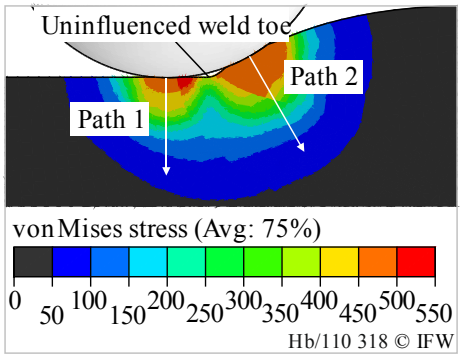

Fig. 7. Local stress state from simulation with the HG13 tool, $p_r = 40$ MPa

As it can be seen in Fig. 7, the von Mises load stress depth profiles of tools HG2 and HG3 act up to a distance to surface of $z = 1$ mm. Regardless of the material state investigated, the bigger ball diameter leads to a higher penetration depth of the load stresses. This is due to higher process forces resulting from bigger projected area of the ball at same rolling pressure. The same behavior can be observed when increasing rolling pressure, which can be explained accordingly. Low rolling pressures of $p_r = 10$ MPa result in an elastic deformation in the BM/HAZ region. This is due to the fact that the combination of applied process force and resulting contact surfaces does not generate a von Mises stress state that exceeds the yield strength of the BM/HAZ region. Especially the FM is responsible for this, acting as a support for the ball. From this it can be concluded that with lower rolling pressures and small ball diameters also for multi tracks no significant influencing of the weld toe will occur.

The derived material parameters are also represented in Fig. 8. It can be seen that the surface near von Mises stress state exceeds the initial yield strength in the BM/HAZ region. The surface near stresses are even higher than the initial yield strength of the FM. This is due to the higher ability of strain hardening of BM/HAZ compared to the FM.

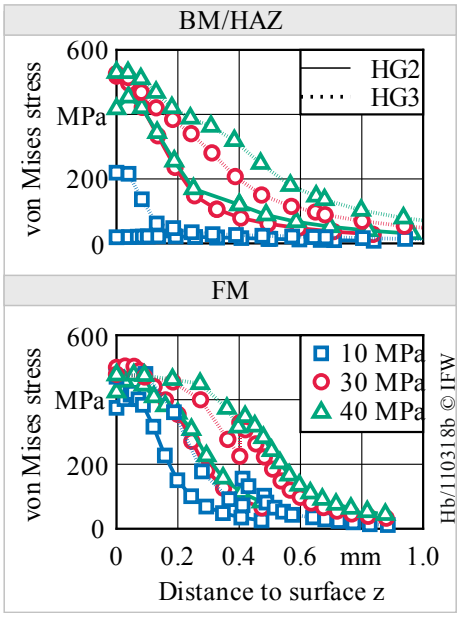

Fig. 8. Von Mises load stress depth profiles for varying ball diameters and rolling pressures

The same behavior regarding a higher penetration depth of acting von Mises load stresses can be observed from the simulations with the HG13 tool, see Fig. 9.

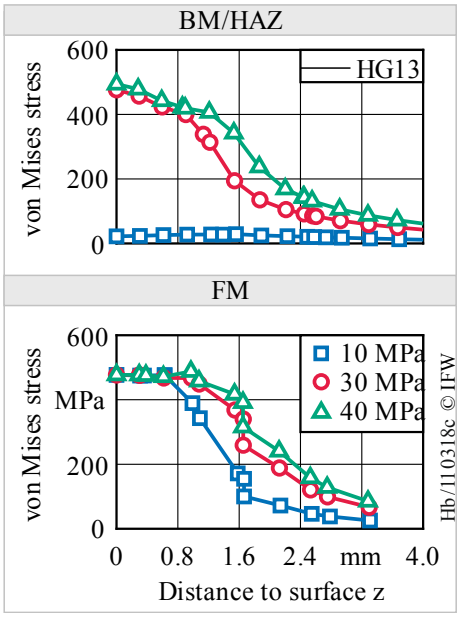

Fig. 9. Von Mises load stress depth profiles for the HG13 tool

In comparison to the HG2 and HG3 tools, the penetration depth of the acting load stresses is higher with a distance to surface of up to z =4 mm. Interestingly the same observations from smaller ball diameters at lower rolling pressures can be made for the bigger ball diameter. Here, the FM also supports the bigger ball. This leads to the conclusion that high rolling pressures for bigger ball diameters are necessary to influence the weld toe, even if the rolling force is 16–40 times higher at a rolling pressure of 10 MPa compared to the one of smaller ball diameters.

4. Conclusions and outlook

This paper deals with the identification of material properties for finite element simulation of the deep rolling process applied to welded joints. From the investigations presented, the following conclusions can be drawn:

- Base material, heat affected zone and filler material of investigated welded joints show different hardening behaviors with different yield strengths and maximum stresses
- Derivation of constitutive behavior for the simulation of the deep rolling process applied to welded joints is therefore necessary due to local support effects of the filler material
- Support effects of the filler material are stronger pronounced for lower rolling pressures regardless of used ball diameters
- Even for higher ball diameters higher rolling pressures are necessary to achieve an influencing of the weld toe
- Multi track simulations are necessary to describe the deformation behavior of the weld toe in detail as no deformation of the weld toe was detectable in the single track simulations presented.

In the future numerical simulations of the deep rolling process applied to welded joints will be extended to multi track simulations, different weld toe geometries and steel grades. A comparison with different constitutive models will verify the necessity of the combined hardening constitutive model used in this study. The results from future numerical studies will be validated by experimental results regarding the influence on the geometry of the weld toe. This will allow for a weld specific deep rolling process design by using FE method.

Acknowledgements

The authors thank the German Federation of Industrial Research Associations (AiF) for the financial support of the project “Deep rolled welds—Increased fatigue strength of welded joints in wind energy by deep rolling”, grant number 20626/N, and the project “Fatigue strength of butt joints of high-strength fine-grained offshore construction steels with and without post-treatment for the construction of offshore wind turbines”, grant number 21496/N. Both projects are part of the program for promoting industrial cooperative research (IGF) based on a decision by the German Bundestag. The projects were initiated and are organized by the Research Association for Steel Application (FOSTA).

References

[1] J. Schubnell, D. Discher, M. Farajian, Determination of the static, dynamic and cyclic properties of the heat affected zone for different steel grades, Materials Testing 61 (2019) 635–642. https://doi.org/10.3139/120.111367.

[2] H. Lieurade, I. Huther, F. Lefebvre, Effect of weld quality and postweld improvement techniques on the fatigue resistance of extra high strength steels, Welding in the World 52 (2008) 106–115.

[3] M.M. Pedersen, O.Ø. Mouritsen, M.R. Hansen, J.G. Andersen, J. Wenderby, Comparison of Post-Weld Treatment of High-Strength Steel Welded Joints in Medium Cycle Fatigue, Welding in the World 54 (2010) 208-217. https://doi.org/10.1007/BF03263506.

[4] P. Delgado, I.I. Cuesta, J.M. Alegre, A. Díaz, State of the art of Deep Rolling, Precision Engineering 46 (2016) 1–10. https://doi.org/10.1016/j.precisioneng.2016.05.001.

[5] T. Kinner-Becker, J. Sölter, B. Karpuschewski, A simulation-based analysis of internal material loads and material modifications in multi-step deep rolling, Procedia CIRP 87 (2020) 515–520. https://doi.org/10.1016/j.procir.2020.02.060.

[6] T. Kinner-Becker, M. Hettig, J. Sölter, D. Meyer, Analysis of internal material loads and Process Signature Components in deep rolling, CIRP Journal of Manufacturing Science and Technology 35 (2021) 400–409. https://doi.org/10.1016/j.cirpj.2021.06.024.

[7] J. Schubnell, Experimentelle und numerische Untersuchung des Ermüdungsverhaltens von verfestigten Kerben und Schweißverbindungen nach dem Hochfrequenzhämmern. Dr.-Ing. Diss., Karlsruher Institut für Technologie (2021).

[8] C. Ernould, J. Schubnell, M. Farajian, A. Maciolek, D. Simunek, M. Leitner, M. Stoschka, Application of different simulation approaches to numerically optimize high-frequency mechanical impact (HFMI) post-treatment process, Welding in the World 63 (2019) 725–738. https://doi.org/10.1007/s40194-019-00701-8.

[9] G.H. Majzoobi, S. Teimoorial Motlagh, A. Amiri, Numerical simulation of residual stress induced by roll-peening, Transactions of the Indian Institute of Metals 63 (2010) 499–504. https://doi.org/10.1007/s12666-010-0071-4.

[10] S. Heikebrügge, B. Breidenstein, B. Bergmann, C. Dänekas, P. Schaumann, Experimental and Numerical Investigations of the Deep Rolling Process to Analyze the Local Deformation Behavior of Welded Joints, Journal of Manufacturing and Materials Processing 6 (2022) 50. https://doi.org/10.3390/jmmp6030050.

[11] D. Trauth, F. Klocke, P. Mattfeld, A. Klink, Time-efficient Prediction of the Surface Layer State after Deep Rolling using Similarity Mechanics Approach, Procedia CIRP 9 (2013) 29–34. https://doi.org/10.1016/j.procir.2013.06.163.

[12] F. Dunne, N. Petrinic, Introduction to computational plasticity, first. publ, Oxford University Press, Oxford (2005).

[13] F. Zaverl Jr., D. Lee, Constitutive relations for nuclear reactor core materials, Journal of Nuclear Materials 75 (1978) 14–19.

[14] M. Wójcik, A. Skrzat, Identification of Chaboche–Lemaitre combined isotropic–kinematic hardening model parameters assisted by the fuzzy logic analysis, Acta Mechanica 232 (2021) 685–708. https://doi.org/10.1007/s00707-020-02851-z.

[15] C.O. Frederick, P.J. Armstrong, A mathematical representation of the multiaxial Bauschinger effect (Reproduction of original 1966 CEGB internal research report), Materials at High Temperatures 24 (2007) 1–26. https://doi.org/10.3184/096034007X207589.

[16] J.L. Chaboche, Time-independent constitutive theories for cyclic plasticity, International Journal of Plasticity 2 (1986) 149–188. https://doi.org/10.1016/0749-6419(86)90010-0.